White Rose Research Online

eprints@whiterose.ac.uk
https://eprints.whiterose.ac.uk
Universities of Leeds, Sheffield and York

Deposited via The University of Sheffield.

White Rose Research Online URL for this paper:
https://eprints.whiterose.ac.uk/id/eprint/90214/

Version: Accepted Version

Article:

Davidson, J., Stone, D., Foster, M. et al. (2016) Measurement and characterisation technique for real-time die temperature prediction of MOSFET-based power electronics. IEEE Transactions on Power Electronics, 31 (6). ISSN: 0885-8993

https://doi.org/10.1109/TPEL.2015.2476557

Reuse
Items deposited in White Rose Research Online are protected by copyright, with all rights reserved unless indicated otherwise. They may be downloaded and/or printed for private study, or other acts as permitted by national copyright laws. The publisher or other rights holders may allow further reproduction and re-use of the full text version. This is indicated by the licence information on the White Rose Research Online record for the item.

Takedown
If you consider content in White Rose Research Online to be in breach of UK law, please notify us by emailing eprints@whiterose.ac.uk including the URL of the record and the reason for the withdrawal request.

UNIVERSITY OF LEEDS University of Sheffield UNIVERSITY of York

This article has been accepted for publication in a future issue of this journal, but has not been fully edited. Content may change prior to final publication. Citation information: DOI 10.1109/TPEL.2015.2476557, IEEE Transactions on Power Electronics

Measurement and Characterisation Technique for Real-Time Die Temperature Prediction of MOSFET-Based Power Electronics

Jonathan N. Davidson, David A. Stone, Martin P. Foster and Daniel T. Gladwin

Abstract—**This paper presents a technique to predict the die temperature of a MOSFET based on an empirical model derived following an offline thermal characterisation. First, a method for the near-simultaneous measurement of die temperature during controlled power dissipation is presented. The method uses a linear arbitrary waveform power controller which is momentarily disconnected at regular intervals to allow the forward voltage drop of the MOSFET's antiparallel diode to be measured. Careful timing ensures the power dissipation is not significantly affected by the repeated disconnection of the power controller. Second, a pseudorandom binary sequence-based system identification approach is used to determine the thermal transfer impedance, or cross coupling, between the dice of two devices on shared cooling using the near-simultaneous measurement and control method. A set of infinite impulse response (IIR) digital filters are fitted to the cross coupling characteristics and used to form a temperature predictor. Experimental verification shows excellent agreement between measured and predicted temperature responses to power dissipation. Results confirm the usefulness of the technique for predicting die temperatures in real time without the need for on-die sensors.**

Index Terms—**Temperature measurement, prediction methods, power control, IIR digital filters, power MOSFETs**

I. INTRODUCTION

KNOWLEDGE of device temperatures in a power electronics system is a valuable asset to the design engineer. However, in many practical systems, system loading and therefore device temperatures can change significantly over time [1]. Equipped with real-time temperatures, the engineer can take steps to predict mechanical failure [2], manipulate the temperature profile of devices to prevent overheating and reduce thermal cycling [3], and implement intelligent cooling control [4]. Design engineers often use the easy-to-measure device case temperature for those purposes, and acquire it using discrete temperature sensors, thermocouples or infra-red sensors. However, the efficacy of these applications would be improved if, instead of relying on case temperature, the temperatures of the semiconductor dice were used. In most cases, it is damage to the die which leads to system failure through mechanisms including die lift-off [5, 6], ruptured wire bond to the die [6] and dopant diffusion [7]. Die temperatures are therefore the variables which should preferably be monitored and controlled within a system. Case temperatures can only be an approximation to die temperature, and the relationship between the two varies with packaging, cooling and input power.

J.N. Davidson, D.A. Stone, M.P. Foster and D.T. Gladwin are with the Department of Electronic and Electrical Engineering, The University of Sheffield, Sir Frederick Mappin Building, Mappin Street, SHEFFIELD S1 3JD, UK (e-mail: Jonathan.Davidson@sheffield.ac.uk; D.A.Stone@sheffield.ac.uk; M.P.Foster@sheffield.ac.uk; D.Gladwin@sheffield.ac.uk).

A number of techniques to measure or infer the die temperature are available, several of which are summarised by Blackburn [8]. For packaged devices, die temperature measurement is usually achieved by measuring a temperature-sensitive electrical property, such as threshold voltage [9], or tunnelling current [10]. However, taking these measurements usually requires the exclusive use of the semiconductor component which makes it challenging to take die temperature readings of an active device in a powered system. If a method for simultaneous measurement can be implemented, it necessarily involves complex circuitry, increasing system cost.

As an alternative, this paper develops a technique to predict the die temperature in real-time without the need for on-system die temperature measurement circuitry. In previous work [11], we proposed a computationally efficient predictor of case temperatures based on an offline characterisation process and real-time power dissipation data. In this work, we extend the technique to predict die temperatures in a working system.

The characterisation process is based on offline power dissipation and temperature measurement (a full description of the method used is provided in section 4). For die temperature measurements, however, the measurement process typically requires exclusive use of the device. Therefore, unless the device is specifically redesigned to incorporate a separate on-die temperature sensor, power dissipation and temperature measurement cannot occur simultaneously. It is therefore necessary to develop a method for die temperature measurement with simultaneous controlled power dissipation. Therefore, this paper develops a near-simultaneous temperature measurement and power controller for a MOSFET die, which is subsequently used in the thermal characterisation of a multiple device system. Following characterisation, a temperature predictor is developed and used to predict the temperature response of the practical system to power input without using the temperature measurement circuitry.

Previous literature has presented methods for temperature prediction. Musallam *et al* [12], for example, present a temperature estimator for a single power MOSFET mounted on a heatsink based on a one-dimensional (1-D) thermal model. By analysing the heat transfer path from the active region through the physical structure of the device, the authors populate a 7th order Cauer network using published device characteristics. The paper reports that the network can be reduced to 3rd order without significant impact on results. Verification is achieved

0885-8993 (c) 2015 IEEE. Personal use is permitted, but republication/redistribution requires IEEE permission. See http://www.ieee.org/publications_standards/publications/rights/index.html for more information.

This article has been accepted for publication in a future issue of this journal, but has not been fully edited. Content may change prior to final publication. Citation information: DOI 10.1109/TPEL.2015.2476557, IEEE Transactions on Power Electronics

using the forward diode voltage drop method (discussed in the present paper) to infer die temperature and shows that a reasonable estimation can be achieved. However, the accuracy of the estimate is limited by the 1-D model, which results in prediction errors during transients. A more general model, not limited by model parameterisation, would therefore be preferable.

Chen *et al* [13] use an alternative method of temperature estimation and modelling. A method based on the computation of the MOSFET's threshold voltage, which can be measured both in transient and steady-state operation, is reported. Using this method, the cooling curve observed at the die is used to parameterise a 3rd order Foster network, which is then used as the basis of a real-time temperature predictor. The authors also make allowances for the model to be updated to account for device ageing. Results show good agreement between predicted results and a real cooling curve. However, the reported system considers only the self-heating of a single device—in the multiple device system analysed in the present work, there are limitations on Foster network accuracy [14]. In addition, complex circuitry is required to measure the transient threshold, meaning the technique is most effective for offline thermal characterisation. A temperature predictor for a multiple device system based on empirical characterisation is therefore developed in the present paper.

This paper is organised as follows: Section 2 describes the circuit topology and calibration procedure for die temperature measurement with near-simultaneous controlled power dissipation. Section 3 describes the experimental set-up. Section 4 reports the procedure and results for thermal characterisation of the system under test. Section 5 presents temperature predictions based on the development of infinite impulse response (IIR) digital filters.

II. DIE TEMPERATURE MEASUREMENT WITH NEAR-SIMULTANEOUS CONTROLLED POWER DISSIPATION

A. *Die temperature estimation from the diode forward voltage drop*

One temperature-sensitive property which can be used to measure the die temperature is the forward voltage drop of a conducting diode, measured as shown in Fig. 1. Precker and da Silva [15] have shown that there is a linear correlation between the voltage drop and the die temperature at a particular bias current. Understanding of this property requires the Shockley diode equation, given in (1), which is the relationship between the forward voltage drop and the conduction current of a p-n junction [18].

$$v_{\mathrm{D}} = \frac{kT}{e} \ln\left(\frac{i}{I_0} - 1\right) \quad (1)$$

Where v_{D} is the forward voltage drop, i is the conduction current, T is absolute junction temperature, I_0 is the reverse leaking current, k is the Boltzmann constant and e is elementary charge. It is clear from this equation that there is a temperature dependency between voltage and current. In addition, I_0 is also temperature dependent [15], resulting in a complex relationship. However, over the range of practical temperatures usually considered for power electronics applications, the relationship is approximately linear. This is due to the temperature dependency of I_0, which is shown in (2) [18].

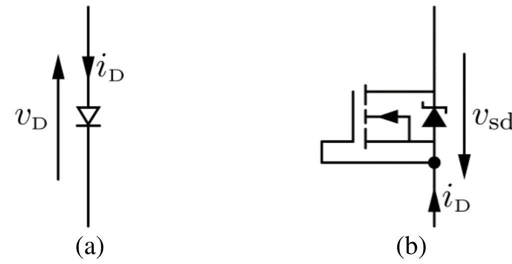

Fig. 1. Voltages and currents relevant to die temperature estimation from the diode forward voltage drop in (a) a standard diode, and (b) the antiparallel diode in a MOSFET

$$I_0 = \alpha T^3 \exp\left(-\frac{E_{\mathrm{g}}}{kT}\right) \quad (2)$$

where α is a constant relating to the diode's construction and materials but not to temperature, E_{g} is the band-gap of the semiconductor and k is the Boltzmann constant. This validity of this equation can be confirmed by observing that I_0 is proportional to the minority carrier concentration (n_{p} or p_{n}) of the junction and therefore, since $n_{\mathrm{p}} \propto n_{\mathrm{i}}^2$ and $p_{\mathrm{n}} \propto n_{\mathrm{i}}^2$, it can be said that $I_0 \propto n_{\mathrm{i}}^2$ [24] where n_{i} is the intrinsic carrier concentration. Since $n_{\mathrm{i}} \propto T^{3/2}$ [24], it can be seen that $I_0 \propto T^3$, as shown in (2). Substituting (2) into (1) and following some manipulation yields

$$v_{\mathrm{D}} = \frac{kT}{e} \cdot \left[\ln\left(\frac{i}{\alpha T^3}\right) + \frac{E_{\mathrm{g}}}{kT}\right] \quad (3)$$

which is approximately linear with gradient $-3k/e$ for large T and constant i. Since working temperatures of power electronics are in excess of 200 K for almost all applications, it is valid to assume that the relationship between v_{D} and T is linear. A full derivation is given in [25].

This property has been used practically for many purposes. Iskrenovic and Mitic [18], for example, use the voltage-temperature relationship to estimate the junction temperature of a diode. By applying very short bursts of constant current to minimise self-heating effects from the measurement system, the diode forward voltage drop can be measured. Because short pulses cause difficultly in accurate sampling of the voltage, the output voltage is low-pass filtered and a bespoke technique is applied for voltage measurement. A quartz crystal oscillator is used for timing and the number of pulses observed between two points along the voltage decay is measured. This gives an estimate of v_{D} which does not require sampling with an analogue-to-digital converter.

Similar techniques can also be applied to other devices which contain a p-n junction, such as seen in the work of Yong-Seok and Seung-Ki [19]. Here it is noted that IGBTs feature an on-state voltage drop, $v_{\mathrm{ce(sat)}}$, which varies with both collector current and junction temperature. The relationship is near linear with a typical 5 kelvins (K) maximum error generated by this assumption. An offline characterisation stage is required to populate physical parameters. These parameters are then used

0885-8993 (c) 2015 IEEE. Personal use is permitted, but republication/redistribution requires IEEE permission. See http://www.ieee.org/publications_standards/publications/rights/index.html for more information.

This article has been accepted for publication in a future issue of this journal, but has not been fully edited. Content may change prior to final publication. Citation information: DOI 10.1109/TPEL.2015.2476557, IEEE Transactions on Power Electronics

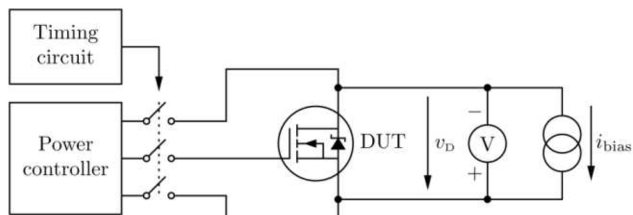

Fig. 2. Functional circuit diagram of MOSFET with heat dissipation and antiparallel diode temperature measurement

online to predict the temperature from the collector current and voltage drop.

MOSFET die temperatures can also be measured using the forward voltage drop across the in-built antiparallel diode present in those devices [20], as shown in Fig. 1(b). In this case, the gate of the MOSFET is shorted to the source in order to prevent current flowing through the channel. An additional current source between the MOSFET's source and drain is used to supply current to the diode so that a voltage drop is evolved.

Care must be taken when estimating temperature from the diode voltage drop because the voltage depends on the excitation current as well as temperature. Unless the effect of both temperature and current are characterised to calibrate the sensor (increasing the complexity of the technique), measurement of the forward voltage drop requires the current through the diode to be a known constant. The measurement therefore requires the device to be put into constant current mode and hence requires exclusive use of the semiconductor die.

Alternative techniques which rely on different physical properties are available that can be used during typical applications, such as through computation of the threshold voltage [13]. However, these techniques require complex circuitry and digital signal processing microelectronics, since devices in active systems undergo high frequency switching which leaves only small measurement periods, and may cause substantial measurement noise. The simplicity of the forward diode voltage technique, which requires only a current source and voltage measurement, is therefore attractive.

B. Proposed circuit

For thermal characterisation, it is necessary to measure the die temperature while simultaneously dissipating power in the die. This presents a significant difficulty since it is not practical to measure temperature while using the device in a high power dissipation mode. To overcome this, a circuit is developed to allow a MOSFET device to be switched between dissipating and measurement modes so that both abilities may be used. This is a temporal division approach whereby the device dissipates power for most of the time, with occasional momentary interruptions for die temperature measurements. By performing the switch rapidly and adjusting power dissipation to account for the non-dissipating periods, power can be controlled with sufficient bandwidth for practical purposes while near-simultaneous temperature measurement can also be achieved. The concept of the circuit is shown in Fig. 2.

A current source, connected across the source and drain of the device under test (DUT), provides a small forward bias

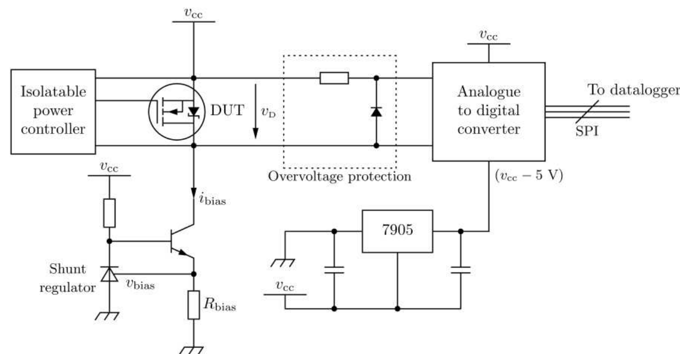

Fig. 3. Isolated antiparallel diode forward voltage measurement (note the upside-down MOSFET, labelled DUT). In this work, the shunt regulator is an LM431 providing a v_{bias} of 2.5 V.

current, i_{bias}. A bias of 10 mA is selected for the IRF510 MOSFET so that the current does not cause significant power dissipation during measurement (i.e. dissipation is typically less than 10 mW during the measurement). A voltmeter is connected across the antiparallel diode to measure the forward voltage drop from which the die temperature is calculated.

An arbitrary waveform power controller [21] is connected to the DUT to control the instantaneous power dissipated in the device. The operation of this controller is described in detail later in this paper. Under normal operation, the power controller determines the dissipation in the device alone by controlling the current and voltage. However, in this arrangement a small proportion of the current bypasses the device and flows through the i_{bias} current source, resulting in a small reduction in power dissipated. The input waveform to the controller is therefore adjusted to correct for this effect. A switch also allows the power controller to be disconnected occasionally to allow the diode voltage drop to be measured.

The measurement sample interval, t_i, (i.e. the time between successive die temperature measurements) is chosen to be much greater than the sample acquisition period so the loss of power dissipation during acquisition has little effect on overall power dissipation. This sample interval must also be sufficiently short such that bandwidth requirements are met (a sample interval of t_i results in a minimum useful frequency of t_i^{-1}). For the work described here, a sample interval of between 0.1 and 1 s is practical since most thermal time constants of the system are significantly longer and enough time is available within the interval for voltage measurement. Very high speed transients, such as those caused by multi-kilohertz switching events, are not considered in this work which instead focusses on steady-state changes in die temperature. At the beginning of the sample interval, the power controller is disconnected and the power loss in the device ceases. The source-drain voltage is therefore determined by the bias current and antiparallel diode. A short settling time delay, t_{delay}, (typically 1-2 ms) is allowed and the voltage acquisition then takes place (over an acquisition period, t_{acq}, of 20 ms in this work). The power controller may then be reconnected until the beginning of the next sample interval. Timing details are given in Fig. 5. By keeping the total disconnect time, t_{discon}, small (for example, less than 20% of the sample interval) and increasing power dissipation by the same proportion, near-simultaneous measurement can be achieved without significantly affecting power dissipation. The

0885-8993 (c) 2015 IEEE. Personal use is permitted, but republication/redistribution requires IEEE permission. See http://www.ieee.org/publications_standards/publications/rights/index.html for more information.

This article has been accepted for publication in a future issue of this journal, but has not been fully edited. Content may change prior to final publication. Citation information: DOI 10.1109/TPEL.2015.2476557, IEEE Transactions on Power Electronics

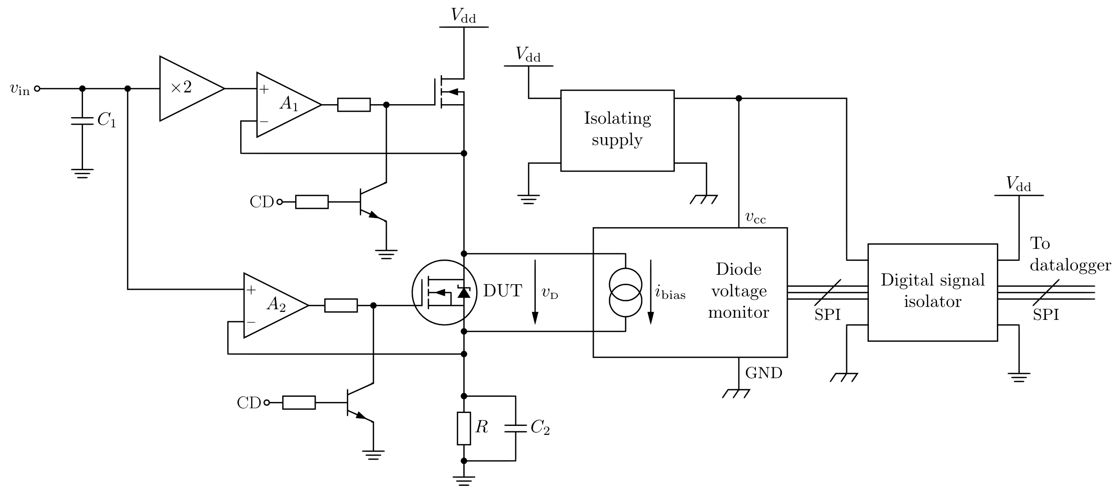

Fig. 4. Power controller circuit for the DUT, with the position of the diode voltage monitor labelled

sample interval and acquisition times are chosen to avoid aliasing by the high frequency die effects, which are present for periods below 10 ms [22].

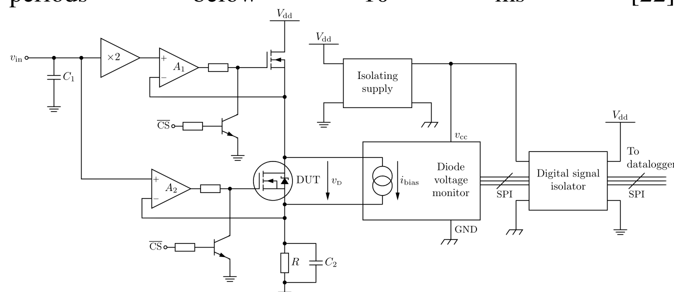

The two parts of this circuit, the power controller and current source, operate in antiparallel and therefore special control and isolation are required. The schematic of the current source and voltage measurement is shown in Fig. 3. The bias current is provided by a constant current sink, controlled by v_{bias} and R_{bias} and transistor ZTX653 which has current gain of over 150. An analogue-to-digital converter (ADC) performs the voltage measurement. Because the absolute voltage at the cathode of the diode is ill-defined, the ADC is instead referenced to the supply voltage, v_{cc}. The negative supply voltage for the ADC is achieved using a 7905 negative voltage regulator which provides a −5 V supply with respect to v_{cc}. The ADC performs differential voltage measurement and sends this data to a datalogger using the serial peripheral interface (SPI) protocol. The ADC is given overvoltage protection to prevent damage when the DUT is being used to dissipate and therefore a large negative voltage would otherwise be applied to the ADC's inputs.

The power controller, shown in Fig. 4, is a modified version of the power controller proposed in [21]. It consists of two operational amplifier-MOSFET pairs in voltage follower configuration. A_2 and R form a current source which causes a current of v_{in}/R to pass through the DUT and R. A_2 additionally controls the source voltage of the DUT, ensuring it is v_{in}. A_1 controls the drain voltage of the DUT, maintaining it at $2v_{\text{in}}$. As a result, the drain-source voltage is v_{in} with a current of v_{in}/R, meaning that the power dissipated in the DUT is

$$p = \frac{v_{\text{in}}^2}{R} \tag{4}$$

A modification is made from the power controller in [21]. In this version, the gates of both the DUT and the voltage controlling MOSFET are grounded when the Controller Disconnect (CD) signal is applied (i.e. $\text{CD} = 1$) thereby providing the grounding function of the switch shown in Fig. 2; the forward voltage drop can then be measured. When power dissipation is desired, CD is not applied and the power controller operates normally. Accounting for this effect, the power dissipated in the circuit is

$$p = \frac{v_{\text{in}}^2}{R}\delta \tag{1}$$

where δ, the duty cycle, is the proportion of time for which the power controller circuit is selected. Decoupling capacitors C_1 and C_2 are added to reduce the noise caused by the rapid switching.

The diode voltage monitor is powered from an isolated power supply to allow the DUT voltage to float freely with operating conditions. A digital signal isolator is used to couple the SPI output of the voltage monitor ADC to the unisolated datalogger so that measurements can be recorded. The circuit is operated using a microcontroller which times the operation of CD and the sampling of the voltage, and performs voltage to temperature conversions. For precise temperature measurement, a high precision ADC is required. For example, to achieve a precision of ±0.1 K (the background noise observed in the measurements for this paper) with a K-type thermocouple, a precision of at least ±39 μV is required. Using a 5 V ADC, a minimum of 17 bits of resolution is necessary. At this level of precision, economically viable ADCs can perform only a few conversions per second and therefore the accuracy of the conversion technique is important. Sigma-delta conversion, which uses oversampling to reduce the complexity of quantisation, is the preferable form of conversion because it is less sensitive to aliasing noise [23].

A simplified timing diagram is given in Fig. 5. For most of the time, the circuit operates in power dissipation mode with $V_{\text{ds}} = v_{\text{in}}$ and $I_{\text{d}} \approx v_{\text{in}}/R$. At the beginning of the measurement

0885-8993 (c) 2015 IEEE. Personal use is permitted, but republication/redistribution requires IEEE permission. See http://www.ieee.org/publications_standards/publications/rights/index.html for more information.

This article has been accepted for publication in a future issue of this journal, but has not been fully edited. Content may change prior to final publication. Citation information: DOI 10.1109/TPEL.2015.2476557, IEEE Transactions on Power Electronics

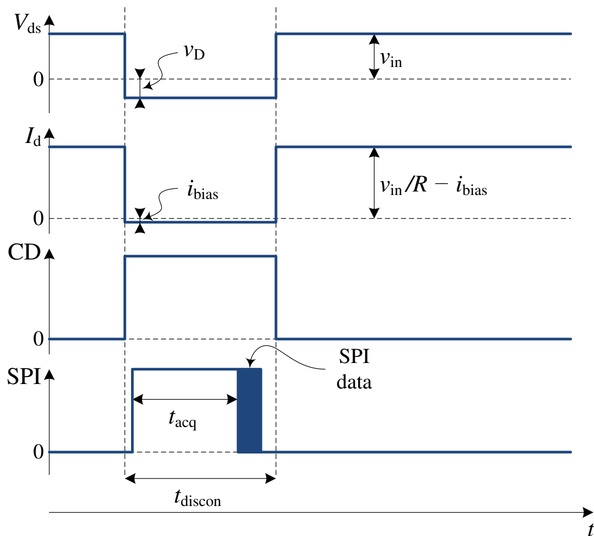

Fig. 5. Timing diagram for MOSFET heat dissipation and die temperature measurement

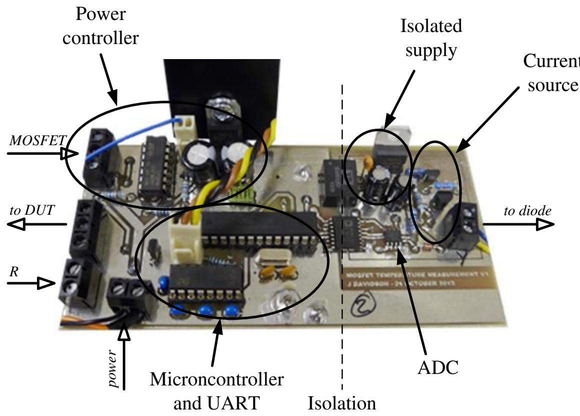

Fig. 6. Practical implementation of the die temperature measurement and dissipation controller

interval, the power controller is disconnected and the antiparallel diode determines the voltage. The diode voltage, v_D, is measured after a short settling time by activating the ADC for a period of t_{acq}. Once acquisition is complete, the SPI data is read and the DUT returns to power dissipation mode.

The measurement system was implemented using IRF510 power MOSFETs, ZTX653 bipolar transistors, an LM431 shunt regulator and an MCP3553 22-bit, 17 ms ADC. The sample interval (t_i) was 200 ms and a total disconnect time (t_{discon}) was 20 ms, giving $\delta = 0.9$. The practical implementation of the control circuit is shown in Fig. 6.

C. Sources of error

The errors in the design can be divided into two types: errors in setting i_{bias}, and errors in setting power dissipation. Errors in i_{bias} are mainly due to the accuracy of R_{bias}, v_{bias} and the gain of the current source transistor and therefore low tolerance components should be selected. Additionally, a high gain transistor should be used to reduce the difference between the collector and emitter currents. However, as long as these sources of error are consistent between calibration and characterisation, which is likely if the ambient temperature is consistent, then i_{bias} will also be consistent.

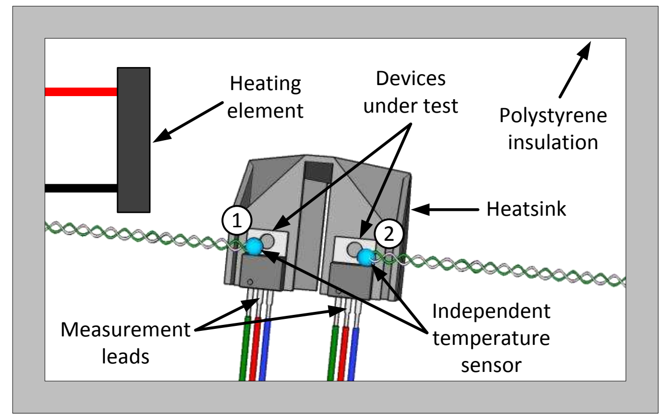

Fig. 7. Calorimeter

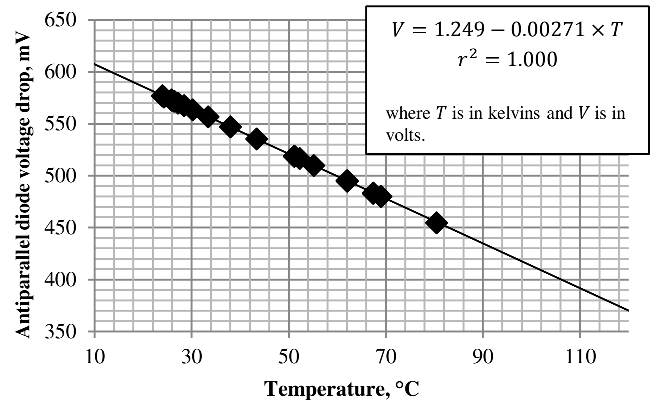

Fig. 8. Practical results of antiparallel diode measurement for MOSFET 1 with line of best fit shown. The equation of the line and the Pearson product-moment correlation coefficient (r) are shown.

The true power dissipation can be calculated from $i_d v_{ds}$ where i_d and v_{ds} are accurately measured. Since i_d depends on the accuracy of R and voltage follower A_3, and v_{ds} depends on the tolerance of resistors R_A and accuracy of op-amps A_1 and A_2, high performance and low tolerance components must be selected in a practical implementation. Power resistor R must also be low tolerance with reduced temperature sensitivity as it directly affects power dissipation, as shown in (4). The effect of temperature sensitivity can be reduced by maintaining R at a constant temperature. The gain, input offset voltage and slew rate of the op-amps introduce an offset voltage between the desired and actual output voltage and therefore high performance op-amps are required. The dynamic response of the circuit can also lead to error if the transient response to the controller being connected is not sufficiently rapid. For the implementation used in this paper, based on the LM324 operational amplifier, the power has a rise time of 11 μs. This is small compared to the period of 200 ms.

D. Calibration

Before the system can be used for measurement, it must be calibrated to determine the gradient and intercept of the relationship between temperature and forward voltage drop. To achieve this calibration, the DUT is placed in a calorimeter. The

0885-8993 (c) 2015 IEEE. Personal use is permitted, but republication/redistribution requires IEEE permission. See http://www.ieee.org/publications_standards/publications/rights/index.html for more information.

This article has been accepted for publication in a future issue of this journal, but has not been fully edited. Content may change prior to final publication. Citation information: DOI 10.1109/TPEL.2015.2476557, IEEE Transactions on Power Electronics

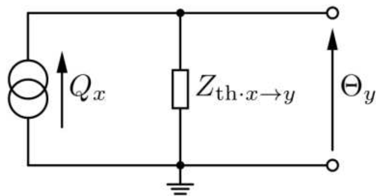

Fig. 9. Norton equivalent electrical circuit between heat dissipation point x and temperature measurement point y.

temperature inside of the calorimeter is controlled by a separate heating element (a power resistor) so that the temperature inside the chamber is uniform after the passing of transient effects. A thermocouple is attached to the DUT to provide an independent temperature reading for the calibration. This paper applies the measurement technique to two devices on shared cooling and therefore two power controllers and DUTs are calibrated in parallel, as shown in Fig. 7.

The power controller was used for voltage measurement with MOSFET power dissipation set to zero. The interior of the chamber is heated to a series of temperatures in turn and the forward voltage drop of the antiparallel diode and the actual chamber temperature is measured at each. A settling time is permitted at each new temperature to ensure the die and case temperatures of the MOSFET are equal. Fig. 8 shows the measured relationship between the case temperature measured by the thermocouple and the diode voltage drop of device 1. The relationship is highly linear, as suggested by (3). The line of best fit is shown, which has a correlation coefficient, r^2, of 1.000, demonstrating this linearity. This relationship can subsequently be used to convert measured voltages to real die temperatures.

III. EXPERIMENTAL ARRANGEMENT

The experimental rig consisting of two MOSFETs mounted on shared cooling, which was shown in Fig. 6, was used for experimental verification. The rig was removed from the calorimeter and tested in free air with only natural convection. This demonstrator system, which has multiple devices thermally coupled to each other, is considered because it is representative of real-world situations. For instance, a power module typically consists of several power devices on a common backplate. Power dissipation in one device causes heating both in that device (due to the thermal auto coupling) and in nearby devices (due to cross coupling).

IV. CHARACTERISATION OF THE THERMAL CROSS COUPLING

Typically, measuring the die temperature in an active system is difficult and involves additional circuitry or sensors. When a measurement system is implemented, it represents an increased system cost. Instead, this paper develops a method to predict the die temperature for real-time power dissipation in a system, following initial characterisation of the thermal system.

In previous work [11], we used a Norton circuit-based cross coupling characterisation method to predict device surface temperatures. This technique is applied here to predict die temperatures. The Norton equivalent circuit models the relationship between the temperature at some point, y, and the power dissipation at the junction of device x, as shown in Fig.

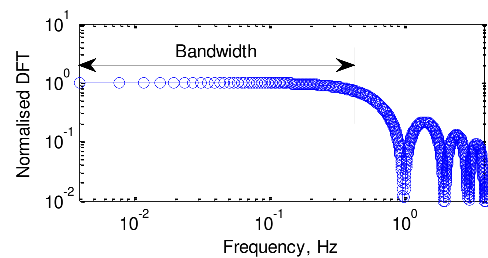

Fig. 10. Bode plot of the frequency content of an 8-bit PRBS calculated using the DFT

9. The thermal transfer impedance, or *cross coupling*, between these points is equivalent to the Norton shunt impedance. For a system with several devices and several points to predict the temperature at, superposition theory may be used. This leads to the construction of a frequency-dependent cross coupling matrix, $\boldsymbol{Z}_{\mathbf{th}}(\mathrm{j}\omega)$, related to temperature and power by (6) and (7).

$$\boldsymbol{\Theta}(\mathrm{j}\omega) = \boldsymbol{Z}_{\mathbf{th}}(\mathrm{j}\omega) \cdot \boldsymbol{Q}(\mathrm{j}\omega) \tag{6}$$

$$\boldsymbol{Z}_{\mathbf{th}} = \begin{pmatrix} Z_{\mathrm{th}\cdot 1\rightarrow 1} & \cdots & Z_{\mathrm{th}\cdot n\rightarrow 1} \\ \vdots & \ddots & \vdots \\ Z_{\mathrm{th}\cdot 1\rightarrow m} & \cdots & Z_{\mathrm{th}\cdot n\rightarrow m} \end{pmatrix}; \quad \boldsymbol{\Theta} = \begin{pmatrix} \Theta_1 \\ \vdots \\ \Theta_m \end{pmatrix}; \quad \boldsymbol{Q} = \begin{pmatrix} Q_1 \\ \vdots \\ Q_n \end{pmatrix} \tag{7}$$

Where $\Theta_x(\mathrm{j}\omega)$ and $Q_x(\mathrm{j}\omega)$ are the frequency-domain temperature representations of temperature and power respectively at point, x, and $Z_{\mathrm{th}\cdot x\rightarrow y}(\mathrm{j}\omega)$ is the cross coupling between points x and y. Equation (6) can then be used to calculate the frequency domain temperature response of a system from the Fourier transform of the input power.

A. Pseudorandom binary sequences

To determine the cross coupling between each pair of devices, a pseudorandom binary sequence (PRBS) technique is used. The PR BS is a special signal, produced using linear shift feedback registers, which is notable for its almost uniform frequency content over its bandwidth [16]. The discrete Fourier transform (DFT) of an 8-bit PRBS is shown in Fig. 10.

A PRBS can be used as an excitation signal for a form of band-limited white noise system identification. By applying the PRBS as a power input to a system, measuring the temperature response and finding the quotient of the two in the frequency domain, the cross coupling between the input and output points is determined as shown in (8).

$$Z_{\mathrm{th\cdot x\rightarrow y}}(\omega) = \frac{\mathcal{F}\left(\theta_{\mathrm{y}}(t)\right)}{\mathcal{F}\left(q_{\mathrm{x}}(t)\right)} = \frac{\Theta_{\mathrm{y}}(\omega)}{\mathrm{Q_x}(\omega)} \tag{8}$$

Where $\theta_{\mathrm{y}}(t)$ and $q_{\mathrm{x}}(t)$ are the time domain representations of the temperature at point y and the power dissipated at point x, respectively and $\mathcal{F}$ is the discrete Fourier transform. The valid bandwidth of the determined response depends on the clock frequency and length of the PRBS. For an n-bit sequence, clocked at f_{P}, the valid band is (from [17])

0885-8993 (c) 2015 IEEE. Personal use is permitted, but republication/redistribution requires IEEE permission. See http://www.ieee.org/publications_standards/publications/rights/index.html for more information.

This article has been accepted for publication in a future issue of this journal, but has not been fully edited. Content may change prior to final publication. Citation information: DOI 10.1109/TPEL.2015.2476557, IEEE Transactions on Power Electronics

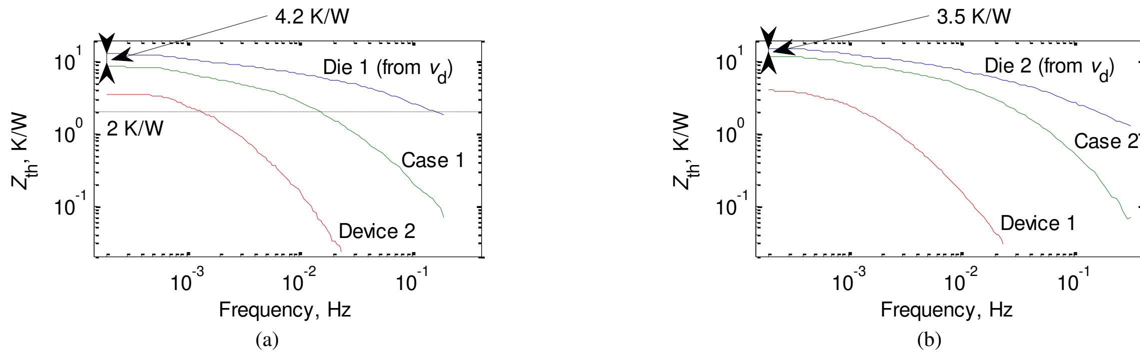

Fig. 11. Cross coupling Bode plots from (a) device 1 and (b) device 2

$$\frac{f_{\mathrm{P}}}{2^n - 1} \leq f \leq \frac{f_{\mathrm{P}}}{2.3} \tag{9}$$

B. *Thermal cross coupling characterisation*

The PRBS characterisation was used to determine the cross coupling between the devices in the experimental arrangement described in section 3. To achieve sufficient bandwidth, three 8-bit PRBS power inputs were used in turn, clocked at 0.05 Hz, 0.5 Hz and 2.5 Hz respectively. To reduce the effect of noise, several repeats of each sequence were averaged together. This resulted in a valid frequency range of 0.20 mHz to 190 mHz. In the cross coupling case, the upper frequency was reduced to 24 mHz since noise was a problem above this frequency. This has negligible effect on results because the thermal impedance is small above this frequency.

A microcontroller-based PRBS waveform generator was used as an input to the power controller to apply each of the signals. Once running, a settling period was allowed for any transient effects to pass before the measurements were taken. Temperature results were taken for each device using the antiparallel diode and also from the attached thermocouple to measure the surface cross coupling. The results for each cross coupling were joined together to produce a single characteristic and noise affected portions of the results were excised. The cross coupling results for the experimental arrangement are shown in Fig. 11.

The curves show the system's thermal cross coupling characteristics. The higher the cross coupling, Z_{th}, the greater the temperature response to a given amplitude of power dissipation at the frequency shown on the horizontal axis. It is therefore expected that the closer the point of power dissipation to the point of temperature measurement, the higher the cross coupling will be. For high frequency perturbations, the thermal system averages out changes in power and therefore the cross coupling is reduce, while at very low frequencies, the thermal capacitance is insignificant compared to the thermal resistance and therefore there is little change in cross coupling below a certain frequency. As the point of temperature measurement moves closer to the power source, the cross coupling remains does not reduce significantly until progressively higher frequencies because, in general, the thermal capacitance reduces relative to the thermal resistance the nearer the measurement is to the power source. It is the particular shapes and properties of these curves which describe the thermal characteristics of the system.

Results show that the thermal coupling is highest at the die under test, with a substantial reduction between die and case. The device datasheet [26] quotes 3.5 K/W as the junction-to-case thermal resistance; the values apparent from Fig. 11 are 4.2 and 3.5 K/W for devices 1 and 2 respectively. The discrepancy highlights the difference between devices and variations in case temperature measurement caused by the precise positioning of sensors, which affects thermal impedance results. The auto coupling (i.e. the cross coupling between a device and itself) shows increased impedance compared to the die-to-case coupling at low frequency and has a reduced roll off at higher frequencies. The die temperature is therefore significantly more sensitive to high power transients, which have high magnitude at higher frequencies, than the case temperature. The extent of the difference between the die and case characteristics highlights the size of error that can be caused by using the case temperature as an indicator of die temperature instead of using the die temperature itself.

The cross coupling between the two devices is significantly lower than the die-to-case coupling. This is expected because the cross coupling reduces with distance. The cross coupling has a similar roll off to, but lower corner frequency than, the die-to-case coupling. It therefore has reduced sensitivity to high frequency inputs. For example, the thermal coupling between the die of device 1 and (i) itself at 160 mHz, (ii) the case of device 1 at 15 mHz, and (iii) the other device at 1.4 mHz are identical at 2.0 K/W. There is therefore an order of magnitude difference between the frequency required to cause a given perturbation at the die and the frequency required at the case. A further order of magnitude is required for the same effect at the other device. For systems with high frequency components in their power waveforms, this means that larger temperature perturbations are seen at the die compared to the case. In addition, the higher DC component in the auto-coupling case causes a higher average temperature. Real-time prediction of the die temperature is therefore important in cases of rapidly varying power dissipation.

V. TEMPERATURE PREDICTION

Using the characterisation results, the temperature of the devices can be predicted using (6). However, this equation is based on frequency domain mathematics. The power waveforms must therefore be converted to the frequency domain before the calculation and the temperature response

0885-8993 (c) 2015 IEEE. Personal use is permitted, but republication/redistribution requires IEEE permission. See http://www.ieee.org/publications_standards/publications/rights/index.html for more information.

This article has been accepted for publication in a future issue of this journal, but has not been fully edited. Content may change prior to final publication. Citation information: DOI 10.1109/TPEL.2015.2476557, IEEE Transactions on Power Electronics

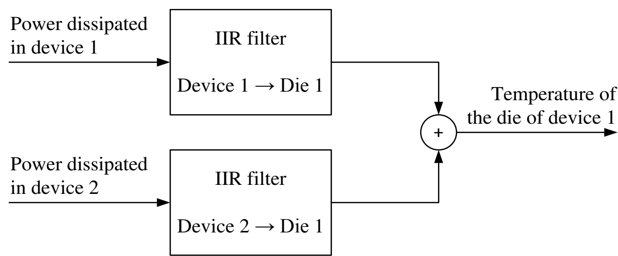

Fig. 12. Method for calculating die temperature predictions from power dissipation data

converted back to the time domain. An approach using (6) requires considerable computational power and is difficult to embed on a microcontroller for real-time operation. An alternative method is therefore required.

A. Temperature prediction using infinite impulse response (IIR) filters

One computationally efficient method to predict the temperatures is to transform (6) into the z-domain, as shown in (10) and (11).

$$\mathcal{Z}\{\boldsymbol{\Theta}(\mathrm{j}\omega)\} = \mathcal{Z}\{\boldsymbol{Z}_{\mathbf{th}}(\mathrm{j}\omega)\} \cdot \mathcal{Z}\{\boldsymbol{Q}(\mathrm{j}\omega)\} \qquad (10)$$

$$\boldsymbol{\Theta}(z) = \boldsymbol{Z}_{\mathbf{th}}(z) \cdot \boldsymbol{Q}(z) \qquad (11)$$

Where z is the $\mathcal{Z}$-operator variable. If the transformation to the $\mathcal{Z}$-domain produces $\boldsymbol{Z}_{\mathbf{th}}(z)$ where each element can be expressed as a low-order rational function in z^{-1}, then the calculation of $\boldsymbol{\Theta}(t)$ can be performed using infinite impulse response (IIR) digital filters. The filter can be implemented as a small number of difference equations, allowing the temperature response to be calculated progressively with low computational requirements suitable for implementation on a microcontroller.

The conversion from $Z_{\mathrm{th}}(\mathrm{j}\omega)$ to $Z_{\mathrm{th}}(z)$ is carried out using the MATLAB function `invfreqz` [27], which uses the Gauss-Newton iterative method to find vectors $\boldsymbol{b}$ and $\boldsymbol{a}$ which minimise the mean square error between the measured frequency response to be fitted, $Z_{\mathrm{th}}(\mathrm{j}\omega)$, and the approximated response of the IIR filter. Vectors $\boldsymbol{b}$ and $\boldsymbol{a}$ contain the polynomial coefficients of z^{-1} for the numerator and denominator of $Z_{\mathrm{th}}(z)$, respectively. The minimisation function is given in (12).

$$\sum_{k=0}^{n_{\mathrm{s}}-1} \left| Z_{\mathrm{th}}(\omega(k)) - \frac{\sum_{\lambda=0}^{G} b_\lambda \exp\left(-\mathrm{j}\lambda\varphi(k)\right)}{1 + \sum_{\lambda=1}^{H} a_\lambda \exp\left(-\mathrm{j}\lambda\varphi(k)\right)} \right|^2 \qquad (12)$$

$$\varphi(k) = \frac{\pi}{\omega_{\mathrm{max}}}\,\omega(k) \qquad (13)$$

$$\omega(k) = \omega_{\mathrm{min}} \left(\frac{\omega_{\mathrm{max}}}{\omega_{\mathrm{min}}}\right)^{\frac{k}{n_{\mathrm{s}}-1}} \qquad (14)$$

where k is the frequency index and n_{s} is the number of samples over which Z_{th} is calculated. For correct weighting of the different frequencies in the minimisation of function (12), a logarithmic spread of frequencies is used between ω_{min} and ω_{max}, which are the minimum and maximum angular frequencies over which Z_{th} is defined, as shown in (14). $\omega(k)$ is the real angular frequency for which $Z_{\mathrm{th}}(\omega)$ is defined. $\varphi(\omega)$ is the angle the frequency makes in the unit circle in the range $0 \leq \varphi \leq \pi$. For both ω and φ, negative frequencies are omitted due to symmetry.

This minimisation strategy uses complex values of the cross coupling, as opposed to the magnitude alone, and therefore fits the filter to both phase and magnitude of the characterisation results. Vectors of length 4 and 7 were chosen for $\boldsymbol{b}$ and $\boldsymbol{a}$ respectively as these values were the smallest that yielded good results. Although the characterisation procedure is computationally intensive, it is performed offline only once per system. In a previous paper [11], we described a similar procedure in detail and successfully demonstrated its application for case temperature predictions.

B. Verification of temperature prediction

The characteristics shown in Fig. 11 are converted to IIR filters using the above procedure. Two IIR filters are required to predict each temperature response because there are two power dissipation sources in the system. Therefore, in order to predict the temperature at device 1, the contribution from device 1 (the auto coupling) and the contribution from device 2 (the cross coupling) are calculated separately and added together to produce the overall response. This arrangement is shown in Fig. 12.

To verify the proposed techniques, both devices in the example system are excited with a power waveform based on the European community's standard driving cycle waveform [28]. This was selected as the test power waveform for both devices because it contains a wide range of levels of power and rates of change. The input power waveform to device 2 was delayed to allow the differences between the auto and cross coupling responses to be identified. A double speed version of the waveform was also used to highlight the effect of rapid power change. For simplicity, the input power is taken as proportional to the velocity parameter in the driving cycle.

The power waveforms were applied to the devices and the die temperature of device 1 was measured. Graph (i) of Fig. 13 shows the predicted and measured temperature response of the die of device 1, with temperatures expressed relative to ambient. Prediction results show excellent agreement with measured temperature as shown by the error in graph (ii). There is no significant difference in accuracy between the results from standard and double rate driving cycle tests shown in Fig. 13(a) and (b) respectively. They have root-mean-square errors between measured and predicted results of 2.3 K and 1.8 K for the standard and double rate power inputs, respectively. When there is a rapid temperature change, errors are greatest due to a delay in the predictor's response. For thermal cycling and lifetime assessment this is not a significant issue because the correct peak temperatures are calculated meaning calculations of thermal cycling fatigue and similar properties are not affected.

Graph (iii) shows the temperature response at the die of device 1 due to power dissipation in devices 1 and 2 separately, illustrating the difference between the auto coupling and cross

0885-8993 (c) 2015 IEEE. Personal use is permitted, but republication/redistribution requires IEEE permission. See http://www.ieee.org/publications_standards/publications/rights/index.html for more information.

This article has been accepted for publication in a future issue of this journal, but has not been fully edited. Content may change prior to final publication. Citation information: DOI 10.1109/TPEL.2015.2476557, IEEE Transactions on Power Electronics

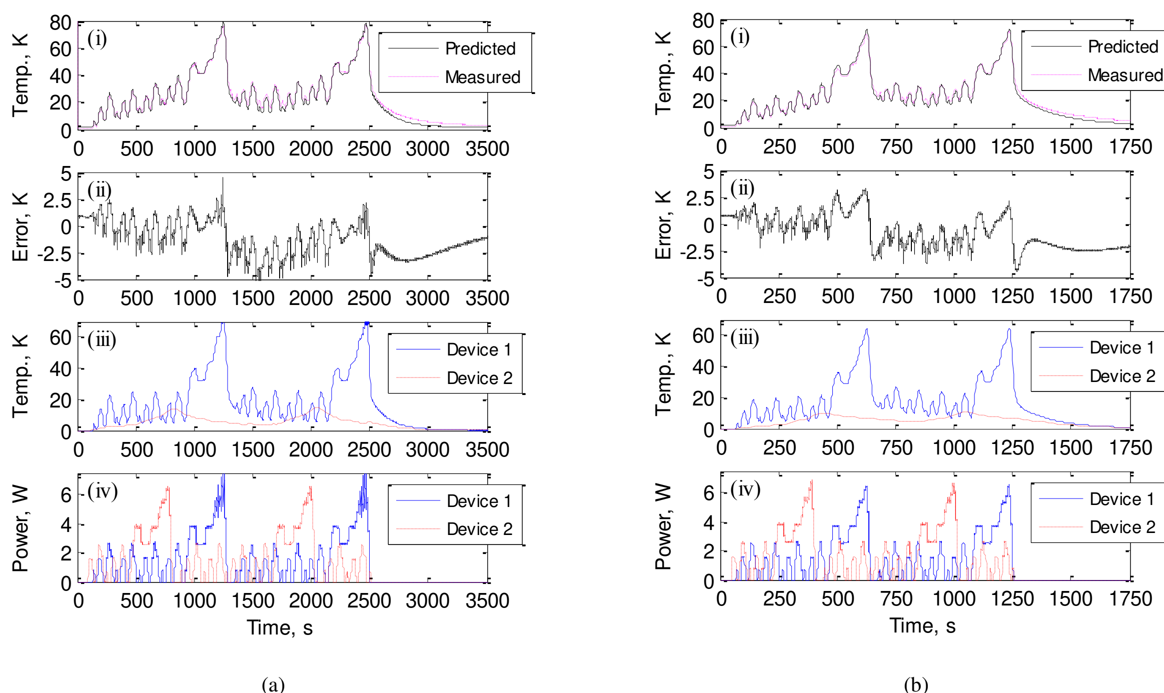

Fig. 13. Predicted and practically measured die temperature response of device 1 at (a) standard rate; and (b) twice standard rate. The graphs show: (i) predicted versus measured temperatures, (ii) error between predicted and measured temperatures, (iii) the temperature response due to dissipation in device 1 and device 2 separately, and (iv) the power input to the devices.

coupling responses. The results are summed together to calculate the prediction in graph (i). The auto-coupling response (the response due to device 1) exhibits high amplitude and rapid reaction to changes in input power. As a result, it dominates the shape of the overall prediction; however, the cross-coupling response (due to device 2) has a slow-changing but important influence on the prediction. By taking into account both devices, an accurate overall temperature response can be produced. Analysis of the case temperature is not normally required for thermal, except to act as a reference to the ambient temperature (for the proposed scheme, such a reference may be taken at any characterised point). If required, an approximation of the heatsink temperature can be calculated from the die-to-case and device-to-device characteristics generated in section 4. For the tests shown in Fig. 13(b), the root-mean-square-error between predicted and measured case temperatures is 1.8 K and 3.4 K for case 1 and case 2 respectively. As with die temperatures, the error is low.

Overall, the results show that the proposed predictor can produce accurate die temperature predictions using an offline empirical cross coupling characterisation. By using a digital filter-based technique, the predictor can be implemented using spare capacity in the microcontroller. Since a microcontroller is required to monitor the temperature responses of devices, and microcontrollers are normally embedded on high-end power converters, as demonstrated by recent commercial controllers [29, 30], this represents negligible additional system cost.

VI. VALUE OF CONSIDERING CROSS COUPLING EFFECTS

Thermal cross coupling effects are an important consideration for engineers when designing a multiple-device system. Especially for space-constrained systems, power dissipation in one device will cause a temperature rise in other devices, particularly the nearest neighbours. This effect is seen most clearly for low frequency perturbations in power dissipation, such as due to changes in load. This effect is in addition to the perturbation caused by high frequency switching. One practical scenario would be a power converter for an electric vehicle where the load is significantly increased during an overtaking manoeuvre.

For cross coupling effects, there will be no significant difference between the resulting temperature rise at the junction of the remote device compared to its case temperature. However, since the die temperature characteristics are already characterised for the thermal auto coupling, there is no significant additional effort required to simultaneously characterise the cross coupling. Therefore, although the die temperature changes rapidly with device dissipation, the temperature of nearby devices also changes more slowly with changes in load. Since these steady-state effects impact the die temperature of all devices, they cannot be neglected if accurate temperature predictions are required. This is particularly relevant for small systems such as power modules where the cross coupling is greatest. In addition, the particular placement of devices on a heatsink impacts on the level of cross coupling between each pair of devices.

In the present work, although the temperature change due to cross coupling is smaller than the auto coupling effect, it nevertheless accounts for 9.3% ($t = 628$ s, Fig. 13(b)) of the total junction temperature at peak temperature, and up to 58% ($t = 464$ s, Fig. 13(b)) at lower temperatures. If this temperature increase is neglected, the predicted temperature would have a significant error. Neglecting cross coupling would therefore represent a significant problem at high temperatures

0885-8993 (c) 2015 IEEE. Personal use is permitted, but republication/redistribution requires IEEE permission. See http://www.ieee.org/publications_standards/publications/rights/index.html for more information.

This article has been accepted for publication in a future issue of this journal, but has not been fully edited. Content may change prior to final publication. Citation information: DOI 10.1109/TPEL.2015.2476557, IEEE Transactions on Power Electronics

where under-prediction could lead to device damage. Although the process of characterising cross-coupling is complex, it is conducted in parallel with the characterisation of the auto coupling and uses the same techniques and measurement data. It therefore represents a modest increase in complexity which is justified by the improved accuracy offered by results.

VII. CONCLUSION

A technique that allows the control of power dissipation in a power MOSFET with simultaneous measurement of die temperature has been presented. The technique uses the forward voltage drop of the antiparallel diode to infer the die temperature. Following calibration of two devices on a shared heatsink, the thermal characteristics of the system were derived using a pseudorandom binary sequence technique. It was shown that by fitting IIR digital filters to the characteristics, the temperature response of the semiconductor die to power dissipation in multiple devices can be predicted. Experimental verification shows excellent agreement between the measured and predicted temperatures of a die following dissipation in the form of the European driving cycle. Results confirm that this technique can be used to predict die temperatures in cross coupled system without the need for complicated circuitry or on-die sensors.

REFERENCES

[1] K. Ma, M. Liserre, F. Blaabjerg and T. Kerekes, '*Thermal Loading and Lifetime Estimation for Power Device Considering Mission Profiles in Wind Power Converter*', IEEE Transactions on Power Electronics, 30, (2), pp. 590-602, Feb 2015
[2] D. Hirschmann, D. Tissen, S. Schroder and R. W. de Doncker, '*Reliability Prediction for Inverters in Hybrid Electrical Vehicles*', IEEE Transactions on Power Electronics, 22, (6), pp. 2511-2517, November 2007
[3] D. A. Murdock, J. E. R. Torres, J. J. Connors and R. D. Lorenz, '*Active thermal control of power electronic modules*', IEEE Transactions on Industry Applications, 42, (2), pp. 552-558, 2006
[4] B. Wrzecionko, D. Bortis and J. W. Kolar, '*A 120°C Ambient Temperature Forced Air-Cooled Normally-off SiC JFET Automotive Inverter System*', IEEE Transactions on Power Electronics, 29, (5), pp. 2345-2358, 2014.
[5] K. B. Pedersen and K. Pedersen, '*Bond wire lift-off in IGBT modules due to thermomechanical induced stress*', Power Electronics for Distributed Generation Systems (PEDG), pp.519-526, June 2012
[6] R. Wu, F. Blaabjerg, H. Wang and M. Liserre, '*Overview of catastrophic failures of freewheeling diodes in power electronic circuits*', Microelectronics Reliability, 53, (9)–(11), pp. 1788-1792, 2013
[7] D. J. Cheney, E. A. Douglas, L. Liu, C.-F. Lo, B. P. Gila, F. Ren and S. J. Pearton, '*Degradation mechanisms for GaN and GaAs high speed transistors*', Materials, 5, (12), pp. 2498-2520, 2012
[8] D. L. Blackburn, '*Temperature measurements of semiconductor devices - a review*', in Proc. Semiconductor Thermal Measurement and Management Symposium, pp. 70-80, 2004
[9] Y. Avenas, L. Dupont and Z. Khatir, '*Temperature Measurement of Power Semiconductor Devices by Thermo-Sensitive Electrical Parameters—A Review*', IEEE Transactions on Power Electronics, 27, (6), pp.3081-3092, 2012
[10] Y.-H. Shih, S.-R. Lin, T.-M. Wang and J.-G.Hwu, '*High sensitive and wide detecting range MOS tunneling temperature sensors for on-chip temperature detection*', IEEE Transactions on Electron Devices, 51, (9), pp. 1514-1521, 2004
[11] J. N. Davidson, D. A. Stone, and M. P. Foster, (In Press) 'Real-time prediction of power electronic device temperatures using PRBS-generated frequency-domain thermal cross-coupling characteristics', IEEE Transactions on Power Electronics, accepted June 2014
[12] M. Musallam, P. P. Acarnley, C. M. Johnson, L. S. Pritchard and V. Pickert, '*Open loop real-time power electronic device junction temperature estimation*', IEEE International Symposium on Industrial Electronics, pp.1041-1046 vol. 2, May 2004
[13] H. Chen, B. Ji, V. Pickert and W. Cao, '*Real-Time Temperature Estimation for Power MOSFETs Considering Thermal Aging Effects*', IEEE Transactions on Device and Materials Reliability, 14, (1), pp. 220-228, 2014
[14] J.N. Davidson, D.A. Stone and M.P. Foster, '*Required Cauer network order for modelling of thermal transfer impedance*', Electronics Letters, 50, (4), pp. 260-262, February 2014
[15] W. J. Precker and M. A. da Silva, 'Experimental estimation of the band gap in silicon and germanium from the temperature–voltage curve of diode thermometers', American Journal of Physics, 70, (11), pp. 1150-1153, 2002
[16] W.D.T. Davies, '*System identification for self-adaptive control*', London: Wiley-Interscience, pp. 44-88, 1970
[17] J. N. Davidson, D. A. Stone, M. P. Foster and D. T. Gladwin, '*Improved bandwidth and noise resilience in thermal impedance spectroscopy by mixing PRBS signals*', IEEE Transactions on Power Electronics, 29, (9), pp. 4817-4828, September 2014
[18] P. S. Iskrenovic and D. B. Mitic, '*Temperature measurement by means of semiconductor diode in pulse mode*', Review of Scientific Instruments, 63, pp. 3182-3184, 1992.
[19] K. Yong-Seok and S. Seung-Ki, 'On-line estimation of IGBT junction temperature using on-state voltage drop', in Industry Applications Conference, pp. 853-859 vol.2, 1998
[20] Z. Jakopovic, Z. Bencic, and F. Kolonic, "Important properties of transient thermal impedance for MOS-gated power semiconductors," in *IEEE International Symposium on Industrial Electronics*, pp. 574-578 vol.2, 1999
[21] J. N. Davidson, D. A. Stone and M. P. Foster, '*Arbitrary waveform power controller for thermal measurements of semiconductor devices*', Electronics Letters 48, (7), pp. 400-402, March 2012
[22] J. L. Shue and H. W. Leidecker, '*Power MOSFET Thermal Instability Operation Characterization Support*', Virginia, USA: National Aeronautics and Space Administration, NASA/TM-2010-216684, April 2010.
[23] B. E. Boser and B. A. Wooley, "The design of sigma-delta modulation analog-to-digital converters," *IEEE Journal of Solid-State Circuits,* 23, pp. 1298-1308, 1988.
[24] B. G. Streetman and S. K. Banerjee, '*Solid state electronic devices*', New Jersey: Prentice Hall, Sixth edition, 2006
[25] J. N. Davidson, 'Advanced thermal modelling and management techniques to improve power density in next generation power electronics', Ph.D. thesis, Dept. Electron. and Elect. Eng., Univ. of Sheffield, Sheffield, UK, 2015
[26] Vishay, '*IRF510, SiHF510 Power MOSFET datasheet*', Malvern, USA: Vishay Siliconix, March 2011
[27] MathWorks (8 July 2013). MATLAB 2013a documentation: invfreqz [Online]. Available: http://www.mathworks.co.uk/help/signal/ref/invfreqz.html
[28] European Community, '*Directive 90/C81/01*', EEC Journal Officiel No. C81, p. 110, 30 March 1990
[29] Microchip, 'New Digitally Enhanced Power Analog Controllers From Microchip Offer Digital Power Supply Flexibility With Easy Analog Control', Chandler, Ariz., USA, 21 October 2014, [Online]. Available: http://www.microchip.com/
[30] S. Sirisukprasert, L. Jih-Sheng; L. Tian-Hua, '*Optimum harmonic reduction with a wide range of modulation indexes for multilevel converters*' IEEE Transactions on Industrial Electronics, 49, (4), pp.875-881, 2002

Jonathan N. Davidson received the M.Eng. degree in electronic engineering and the Ph.D. degree in thermal modelling and management from the University of Sheffield, Sheffield, U.K. in 2010 and 2015, respectively.

In 2015 he became a lecturer in multidisciplinary engineering at the University of Sheffield. His research interests include thermal modelling and management of power electronics, and the design and analysis of piezoelectric transformer-based power

0885-8993 (c) 2015 IEEE. Personal use is permitted, but republication/redistribution requires IEEE permission. See http://www.ieee.org/publications_standards/publications/rights/index.html for more information.

This article has been accepted for publication in a future issue of this journal, but has not been fully edited. Content may change prior to final publication. Citation information: DOI 10.1109/TPEL.2015.2476557, IEEE Transactions on Power Electronics

converters.

Dr. Davidson is a member of the Institution of Engineering and Technology.

David A. Stone received the B.Eng. degree in electronic engineering from the University of Sheffield, Sheffield, U.K., in 1984 and the Ph.D. degree from Liverpool University, Liverpool, U.K., in 1989.

He then returned to the University of Sheffield as a member of academic staff specialising in power electronics and machine drive systems. His current research interests are in hybrid-electric vehicles, battery management, EMC, and novel lamp ballasts for low pressure fluorescent lamps.

Martin P. Foster received the B.Eng. degree in electronic and electrical engineering, the M.Sc. (Eng.) degree in control systems, and the Ph.D. degree for his thesis "Analysis and Design of High-order Resonant Power Converters" from the University of Sheffield, Sheffield, U.K., in 1998, 2000, and 2003, respectively.

In 2003, he became a member of academic staff at Sheffield specialising in power electronic systems and was made Senior Lecturer in 2010 and then Reader in 2014. His current research interests include the modelling and control of switching power converters, resonant power supplies, multilevel converters, battery management, piezoelectric transformers, power electronic packaging, and autonomous aerospace vehicles.

Daniel T. Gladwin received the M.Eng (Hons.) degree in electronic engineering (computer architecture) and the Ph.D. degree in automated control structure design and optimisation using evolutionary computing from the University of Sheffield, Sheffield, U.K. in 2004 and 2009 respectively.

In 2012 he was appointed a lecturer at Sheffield. His active research is into power system control, power electronics, energy storage and management, embedded systems, and intelligent systems.

0885-8993 (c) 2015 IEEE. Personal use is permitted, but republication/redistribution requires IEEE permission. See http://www.ieee.org/publications_standards/publications/rights/index.html for more information.